Indium–Tin–Oxide–Based Transparent Conducting Layers for Highly Efficient Photovoltaic Devices

ARTICLE *in* THE JOURNAL OF PHYSICAL CHEMISTRY C · APRIL 2009

Impact Factor: 4.77 · DOI: 10.1021/jp809011a

9 AUTHORS, INCLUDING:

Sangwook Lee
University of California, Berkeley
77 PUBLICATIONS **1,700** CITATIONS
SEE PROFILE

In-Sun Cho
Stanford University
87 PUBLICATIONS **1,969** CITATIONS
SEE PROFILE

Jung Min Kim
Daejeon University
1,753 PUBLICATIONS **13,169** CITATIONS
SEE PROFILE

Hyunho Shin
Gangneung-Wonju National University
144 PUBLICATIONS **1,453** CITATIONS
SEE PROFILE

Indium−Tin−Oxide-Based Transparent Conducting Layers for Highly Efficient Photovoltaic Devices

Sangwook Lee,[†] Jun Hong Noh,[†] Shin-Tae Bae,[†] In-Sun Cho,[†] Jin Young Kim,[‡] Hyunho Shin,[§] Jung-Kun Lee,[||] Hyun Suk Jung,*[,⊥] and Kug Sun Hong*[,†]

School of Materials Science and Engineering, Seoul National University, San 56-1, Shillim-dong, Kwanak-gu, Seoul 151-744, South Korea, Chemical and Bioscience Center, National Renewable Energy Laboratory, Golden, Colorado 80401, USA, Department of Ceramic Engineering, Kangnung National University, Kangnung, 210-702, South Korea, Department of Mechanical Engineering and Materials Science, University of Pittsburgh, Pittsburgh, Pennsylvania 15260, USA, and School of Advanced Materials Engineering, Kookmin University, Jeongneung-dong, Seongbuk-gu, Seoul 136-702, South Korea

Received: February 29, 2008; Revised Manuscript Received: January 14, 2009

Additional hydrogen (H_2) annealing and subsequent electrochemical treatment are found to make tin-doped indium oxide (ITO)-based photoelectrodes suitable for highly efficient dye sensitized solar cells. The additional H_2 annealing process recovered the electrical conductivity of the ITO film the same as its initial high conductivity, which enhanced the charge collecting property. Moreover, the employment of electrochemical oxidation of TiO_2/ITO photoelectrode improved the energy conversion efficiency of the ITO-based dye-sensitized solar cells (DSSC), higher than that of a conventional FTO-based DSSC. Electrochemical impedance analysis showed that the H_2 annealing process reduced the internal resistance of the cell, i.e., the resistance of the ITO and the Schottky barrier at the TiO_2/ITO interface were reduced, and that the electrochemical treatment recovered the diodelike characteristics of the DSSC by retarding back electron transfer from the photoelectrode to the electrolyte. The present work demonstrates that thermally and electrochemically modified ITO-based photoelectrode is another alternative to the conventionally used FTO-based photoelectrode.

Introduction

Dye-sensitized solar cells (DSSCs) have attracted much attention as promising alternatives to conventional solar energy conversion devices because of their low cost of production and high energy conversion efficiency.[1−4] Transparent conductive oxide (TCO) layers, which collect charge carriers from TiO_2 and transfer them to the external electric circuit, are one of the most important components of a solar cell because low charge collecting efficiency of a TCO layer may deteriorate the cell performance. Therefore, TCO layers have been studied extensively to understand the nature of the TiO_2/TCO interface and to improve the charge collecting efficiency.[5−14]

Because of good electrical conductivity at room temperature and high transparency in the visible range, tin-doped indium oxide (ITO) films have been extensively used as transparent electrodes in electronics and optoelectronics applications, including heaters in windows, sensors, flat panel displays, and solar cells.[15−18] However, ITO films are unfavorable for use in DSSCs because the charge collection properties of ITO films are significantly destroyed after an annealing process in conventional air; photoelectrodes that consist of a TiO_2 film and a TCO layer should be annealed in an oxidizing atmosphere with a temperature over 300 °C to interconnect the TiO_2 nanoparticles, adhere the TiO_2 film to the TCO layer, and remove residual organics from the TiO_2 nanoparticle layer.

The electrical conductivity of ITO originates from free carriers that are generated by the following lattice defects: (i) Sn^{4+} ion in an In^{3+} site and (ii) vacancies in the regular oxygen lattice.[19] The deterioration in conductivity of ITO during annealing has been attributed to oxygen from the atmosphere filling a portion of the oxygen vacancies in the ITO film.[20] Therefore, there have been significant efforts to block the penetration of oxygen into ITO films, for example, by forming a fluorine-doped tin oxide (FTO)/ITO double layer, a SnO_2/ITO double layer, and a TiO_2/antimony-doped tin oxide (ATO)/ITO triple layer.[21−23]

A simple way to conserve the electrical conductivity of ITO films is to anneal them in a reducing H_2 atmosphere, thereby preventing annihilation of oxygen vacancies. In the present study, deteriorated TiO_2/ITO electrode (by oxidation annealing process) was annealed in an H_2 atmosphere in order to generate the oxygen vacancy again, that is, to recover the conductivity of ITO film. However, the TiO_2 film could be also reduced by the H_2 annealing which could decrease the performance of the DSSC by generating defects in the TiO_2 film.[24−28] Therefore, an electrochemical oxidation method to remove defects in TiO_2 while conserving the electrical conductivity of ITO was investigated. The effect of the each process on DSSC performances were systematically examined by impedance analysis. Also, we demonstrate that one can obtain good energy-conversion efficiency for a DSSC that employs ITO as the TCO material.

Experimental Methods

For preparation of the TiO_2 slurry, 6 g of TiO_2 nanoparticles (P25, Degussa), 10 mL of ethanol, 9.6 mL of deionized water, 0.4 mL of acetylacetone, and 2.4 g of polyethylene glycol (PEG, MW 20000) were mixed and ball-milled for 12 h to yield a

* To whom correspondence should be addressed. E-mail: hjung@kookmin.ac.kr (H.S.J.); kshongss@plaza.snu.ac.kr (K.S.H.).
[†] Seoul National University.
[‡] National Renewable Energy Laboratory.
[§] Kangnung National University.
[||] University of Pittsburgh.
[⊥] Kookmin University.

10.1021/jp809011a CCC: $40.75
Published on Web 04/02/2009

homogeneous slurry. TiO_2 films on ITO and FTO conducting electrodes were prepared using a previously reported procedure.[29,30]

The TiO_2-coated electrodes were dried at 80 °C and were then heat-treated using the different conditions detailed below to form photoelectrodes for DSSCs. To remove residual organics and interconnect the nanoparticles, electrodes were annealed at 450 °C for 1 h in O_2; the electrode was designated as electrode A. Generally, TiO_2/ITO electrodes have been annealed in air for DSSC fabrications because O_2 annealing decreases the performance of the DSSC significantly. In the present study, however, the TiO_2/ITO films were annealed in O_2 atmosphere to burn out organics in TiO_2 films completely; because when the air-annealed TiO_2/ITO film was annealed in H_2, the DSSC performance significantly deteriorated rather than improved (Supporting Information). As presented in Supporting Information, the air-annealing process did not fully remove residual organics, which would induce remarkable generation of surface defects on TiO_2 films after the subsequent H_2 annealing process. After the complete decomposition of residual organics in O_2 atmosphere, additional annealing of the electrodes was performed at 350 °C for 2 h in H_2 to recover the conductivity of ITO; the electrode was designated as electrode B. After H_2 annealing, the TiO_2 film of an electrode B was reoxidized electrochemically; the electrode was designated as electrode C. The electrochemical oxidation of the TiO_2 film was carried out using 0.1 M NaOH as the electrolyte and by applying 1 V (vs saturated calomel electrode (SCE)) of electrical potential for 30 min, using a three-electrode system. Electrode C was immersed in the electrolyte solution and acted as an anode, and a Pt plate was used as a counter electrode. To compare DSSCs employing electrodes A, B, and C with a FTO-based DSSC, a TiO_2-coated FTO electrode was annealed at 450 °C for 1 h in O_2, and the electrode was designated as electrode D. Sandwich-type DSSCs were fabricated using a previously reported procedure.[31] The DSSCs composed of electrodes A, B, C, and D were named DSSC A, B, C, and D, respectively. The thickness of the TiO_2 films on the photoelectrodes was approximately 8 μm, as measured by field emission scanning electron microscope (FESEM, model JSM-6330F, Japan). The cross-sectional image shown in Supporting Information confirmed that the TiO_2 thick films were well connected with ITO and FTO films. The amounts of dye molecules adsorbed on the photoelectrodes were also checked by measuring UV−vis spectra of desorbed dye solution from the photoelectrodes. As shown in Supporting Information, all of the samples contained almost similar amounts of dye molecules.

The photovoltaic properties of the fabricated solar cells under the illumination of air mass 1.5 (with Solar simulator; Peccell Technologies, Japan; intensity: 100 mW/cm^2) were measured with the aid of a potentiostat (CHI 608C, CH Instruments, USA). The light intensity of the solar simulator was calibrated with a reference cell (PV Measurements, USA). Electrochemical impedances of the cells were also measured using the potentiostat with 100 mW/cm^2 illumination and by applying open circuit voltage as bias. Surface states of the TiO_2 films were analyzed using X-ray photoelectron spectroscopy (XPS, Model: SIGMA PROBE, ThermoVG, UK). For the V_{oc} decay measurements, the incident light was intercepted in a moment, and the transient decay curve of V_{oc} was monitored during relaxation from an illuminated the quasiequilibrium state to the dark equilibrium state. The data points were collected every 50 ms by using the aforementioned potentiostat. The XPS spectra were acquired using a monochromatic Al K source (100 W), and the binding energy of the Ti (2p) peaks were calibrated with respect to the O (1s) peak from TiO_2 at 530.0 eV. Optical absorption of the ITO electrodes was measured using a UV−vis spectrophotometer (Model: Lambda 35, PerkinElmer, USA). Hall measurements were performed using the van der Pauw method at room temperature to evaluate the electrical properties of the ITO electrodes.

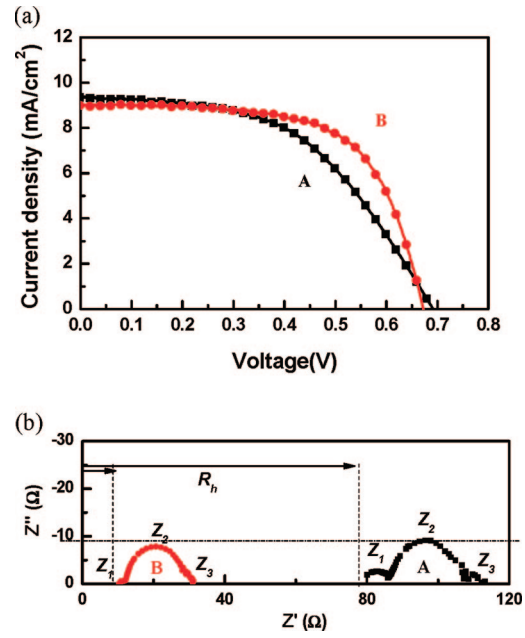

Figure 1. (a) Photocurrent−voltage curves of DSSC A (■) and DSSC B (●); (b) electrochemical impedance spectra of DSSC A (■) and DSSC B (●).

Results and Discussion

When the as-received ITO layer was annealed in oxygen, the electrical resistivity increased from 1.5×10^{-4} to 8.0×10^{-4} Ωcm and the charge carrier concentration decreased from 1.1×10^{21} to 0.21×10^{21} cm^{-3}. After H_2 annealing, the resistivity decreased back to 1.7×10^{-4} Ωcm and the charge carrier concentration increased back to 1.0×10^{21} cm^{-3}, values close to the initial electrical properties. Thus, the H_2 annealing process successfully recovered the electrical properties of the ITO.

Figure 1 shows photocurrent−voltage curves for DSSC A (O_2 annealed) and DSSC B (O_2 annealed and then H_2 annealed). The photovoltaic properties of both DSSC A and DSSC B are summarized in Table 1. Significant improvements in the fill factor (ff) were observed for the additional H_2 annealing step. The overall conversion efficiency increased 18% compared to the H_2 annealing step. This indicates that a loss in energy conversion efficiency of a DSSC is recovered by additional processing of the photoelectrodes using H_2 annealing.

To understand the correlation between the improved cell performance and the internal resistances of the DSSCs, we measured the electrochemical impedance spectra at V_{oc} under AM 1.5. Figure 1b shows the Nyquist plots of DSSC A and DSSC B, which apparently exhibited four impedance elements (R_h, Z_1, Z_2, and Z_3). According to previous studies, the resistance element (R_h) in the high-frequency region (>10^6 Hz) is related to the sheet resistance of the TCO layer. The other three impedance elements (Z_1, Z_2, and Z_3), observed from left to right in the frequency regions of 10^3-10^5 (ω_1), $1-10^3$ (ω_2), and $0.1-1$ (ω_3) Hz, are associated with charge transport at the TiO_2/conducting layer or Pt/electrolyte interfaces (Z_1), the TiO_2/dye/electrolyte interface (Z_2), and the Nernstian diffusion in the

TABLE 1: Cell Parameters of the DSSCs

sample	description	film thickness (μm)/ active area (cm^2)	J_{sc} (mA/cm^2)	V_{oc} (mV)	ff	efficiency (%)
DSSC A	O_2-annealed ITO based DSSC	7.9/0.247	9.4	692	0.50	3.3
DSSC B	H_2/O_2-annealed ITO based DSSC	8.1/0.256	9.0	673	0.65	3.9
DSSC C	H_2/O_2-annealed and electrochemically treated ITO based DSSC	8.0/0.252	9.1	694	0.69	4.4
DSSC D	O_2-annealed FTO based DSSC	8.3/0.248	8.6	702	0.71	4.3

electrolyte (Z_3), respectively.[32−34] As shown in Figure 1b, the Nyquist plots exhibited three prominent differences in impedance elements between DSSC A and DSSC B. First, R_h of DSSC B significantly decreased, compared to that of DSSC A, from 78.8 to 10.4 Ω, indicating that the sheet resistance of the ITO conducting layer was significantly reduced. Given that a decrease in the sheet resistance of the TCO layer boosts ff of a solar cell (Supporting Information), the improved performance of DSSC B is attributed to the reduced sheet resistance (R_h) of the ITO conducting layer after the additional H_2 annealing process. Second, R_1, the resistance component corresponding to Z_1 which is associated with charge transport at the TiO_2/TCO interface or the Pt/electrolyte interface, significantly decreased (from 5.2 to 1.1 Ω) after H_2 annealing. Since the same Pt counter electrode was used for DSSC A and DSSC B, the difference in Z_1 is caused by the enhanced charge injection from TiO_2 to ITO.[14] Figure 2a shows a schematic diagram of the Schottky barrier formed at the junction between ITO and TiO_2. The increase in charge carrier concentration from H_2 annealing increases the optical band gap, which, in turn, increases the Fermi energy level of the ITO. This was confirmed by a blue shift in the UV-absorption edge of reduced ITO, as shown in Figure 2b. According to the Burstein−Moss effect, the lowest states in the conduction band are blocked by occupied donor electrons, which is responsible for the increased optical badgap.[35,36] Therefore, the increase in the optical band gap of ITO (see Figure 2b) implies that the energy states occupied by donor electrons above the conduction band edge were increased, which leads to an increased height of the Fermi energy level above the bottom of the conduction band, i.e., decreasing the difference in Fermi energy levels between ITO and TiO_2.[35] This indicates that the Schottky barrier, $q(\phi'_m-\phi_s)$, and the built-in barrier, $q(\phi'_m-\chi)$, were lowered, as seen in Figure 2a. Therefore, both the reduced Schottky barrier at the TiO_2/ITO interface (monitored by a decrease of Z_1), and the decreased sheet resistance of the ITO conducting layer contributed to improving ff of DSSC B. Lastly, it is noted that R_2, the resistance component corresponding to Z_2, of DSSC B (15.6 Ω) was less than that of DSSC A (18.2 Ω). The decreased R_2 indicates that annealing the TiO_2 film in H_2 facilitated back electron transfer from the TiO_2 nanoparticles to the electrolyte, thereby increasing the recombination rate at the TiO_2/dye/electrolyte interface.[30,36] The increased back electron transfer results from the formation of Ti^{3+} or oxygen vacancy defects on the surface of TiO_2 nanoparticles. The H_2 annealing process has been known to form Ti^{3+} (or oxygen vacancies) on the surface of TiO_2 nanoparticles,[24−27] which act as recombination centers shunting the TiO_2 to the electrolyte.[28] XPS analysis was performed to confirm the formation of surface defects on the H_2/O_2 annealed TiO_2 film (electrode B). As shown in Figure 3, the Ti $2p_{3/2}$ binding energy of the O_2 annealed TiO_2 film (electrode A) was 458.8 eV, indicating that the TiO_2 photoelectrode consists of Ti^{4+} ions.[37] The Ti $2p_{3/2}$ binding energy of the H_2/O_2 annealed TiO_2 film (electrode B) was shifted to a lower energy. This illustrates that the H_2 annealing process reduces the TiO_2 film and generates Ti^{3+} ions, consistent with the electrochemical impedance study.

The additional H_2 annealing process recovered the electrical conductivity of ITO, thereby improving carrier injection from TiO_2 to ITO. However, the reducing conditions of the H_2 annealing process generate defects such as Ti^{3+} ions that could diminish the diodelike characteristic of the DSSC. To remove Ti^{3+} ions from the H_2/O_2-annealed TiO_2 photoelectrode (the TiO_2 film on electrode B) without oxidation of the ITO layer, an electrochemical treatment was adopted, as explained in the

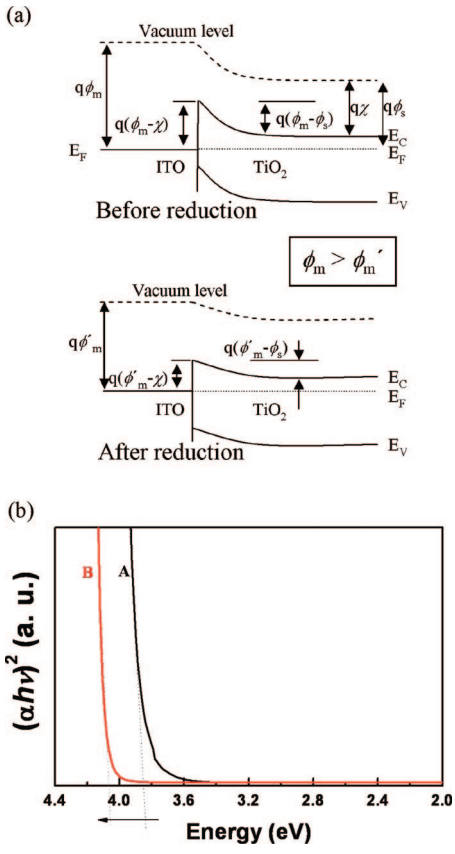

Figure 2. (a) Schematic diagram of the Schottky barrier formed at the junction of ITO and TiO_2; (b) absorption spectra of the ITO layers in electrode A (solid line) and electrode B (dashed line).

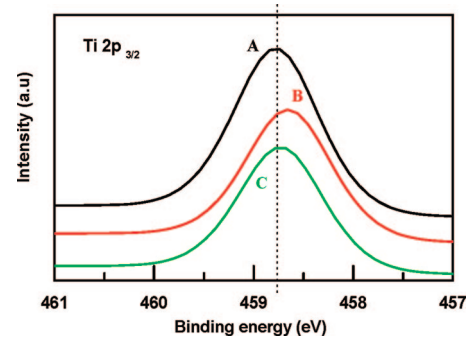

Figure 3. XPS spectra of the TiO_2 films on electrode A (−), B (−), and C (−), for the binding energy region of Ti $2p_{3/2}$.

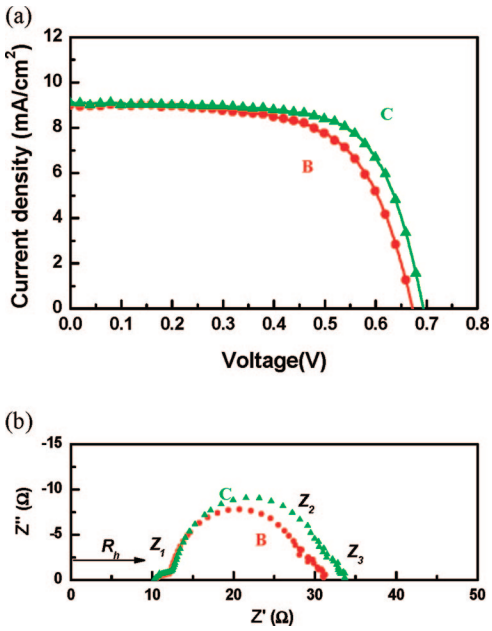

Figure 4. (a) Photocurrent−voltage curves of DSSC B (●) and DSSC C (▲); (b) electrochemical impedance spectra of DSSC B (●) and DSSC C (▲).

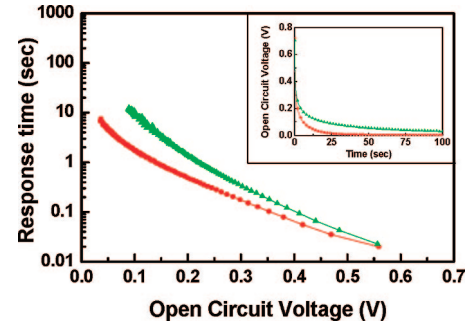

Figure 5. Electron lifetimes for DSSC B (●) and DSSC C (▲) as a function of V_{oc}. The inset shows the open circuit voltage decays for each solar cell.

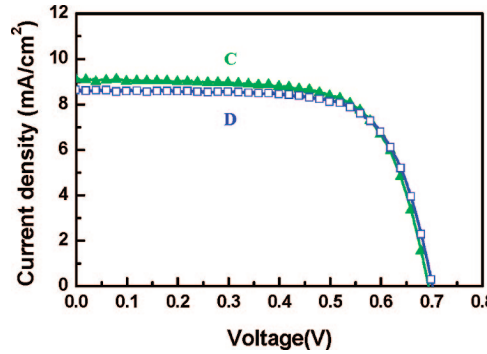

Figure 6. Photocurrent−voltage curves of DSSC C (▲) and DSSC D (□).

experimental methods section. The XPS spectrum of photoelectrode C (H_2/O_2-annealed TiO_2 film, followed by electrochemical treatment) is shown in Figure 3. The Ti $2p_{3/2}$ binding energy shifted to a higher binding energy (458.74 eV), which indicates that Ti^{3+} ions were successfully oxidized to Ti^{4+} ions. These findings demonstrate that the H_2 annealing process generates defects such as Ti^{3+} ions (binding energy peak shifts toward lower energies), but an additional electrochemical treatment recovers the oxidation state of the H_2-annealed TiO_2 film to the fully oxidized state.

To investigate the influence of the electrochemical oxidation of the H_2/O_2-annealed TiO_2/ITO photoelectrode on the performance of the DSSC, photocurrent−voltage curves for DSSC B (employing the H_2/O_2-annealed electrode) and DSSC C (employing the H_2/O_2-annealed and electrochemically treated electrode) were evaluated, and the results are shown in Figure 4. As summarized in Table 1, the overall conversion efficiency of DSSC C increased approximately 13% compared to DSSC B. Specifically, V_{oc} and ff of DSSC C were significantly improved, which can be attributed to the decrease of back electron transfer at the TiO_2/dye/electrolyte interface.

Nyquist plots, shown in Figure 4b, verify the retardation of back electron transfer. R_2 of DSSC C was 18.1 Ω, higher than that of DSSC B (15.6 Ω), while other impedance elements were almost identical. The electrochemical oxidation of TiO_2 film restores the diodelike characteristic of the DSSC, as evidenced by the recovery of the impedance value; R_2 of DSSC C was very similar to that of DSSC A (18.2 Ω). Therefore, the high efficiency of DSSC C results from the elimination of Ti^{3+} ions as well as the enhanced electrical properties of the ITO conduction layer.

To further show retardation of back electron transfer by the electrochemical treatment, the lifetimes of electrons in DSSC B (employing the H_2/O_2-annealed electrode) and DSSC C (employing the H_2/O_2-annealed and electrochemically treated electrode) were obtained (see Figure 5) by measuring the decay of V_{oc} with time (see inset of Figure 5).[38] In comparison with DSSC B, DSSC C showed an increase in carrier lifetime, indicating that the TiO_2 photoelectrode of DSSC C contained fewer recombination sites than DSSC B. Therefore, the impedance spectra (Figure 4b) and the carrier lifetime measurements show that the electrochemical treatment process retards carrier recombination (i.e., back electron transfer) at the surface of the TiO_2 nanoparticles and contributes to improved energy conversion efficiency.

Finally, we compared the performance of DSSC C with that of an FTO-based DSSC (DSSC D). Photocurrent−voltage curves are shown in Figure 6, and important physical parameters are presented in Table 1. The overall conversion efficiency of DSSC C was slightly higher than that of DSSC D. Generally, a good thermal stability of FTO has made it more suitable than ITO for the TCO layer in DSSCs. However, by adapting additional processes involving H_2 annealing and subsequent electrochemical treatment in the present study, ITO-based DSSCs that exhibit comparable or better energy conversion efficiencies compared to FTO-based DSSCs can be fabricated. The excellent photovoltaic performance of ITO-based DSSCs originate from (i) their superior electrical conductivity and (ii) the higher transmittance of the recovered ITO electrode (H_2/O_2-annealed), as shown in Supporting Information.

Conclusions

In the present study, the electrical conductivity of an ITO electrode was returned to a high initial conductivity by applying an additional hydrogen-annealing process. The DSSC with this H_2-annealed ITO electrode demonstrated significantly improved efficiency as compared to the counterpart electrode without H_2 annealing, due to reduced internal resistance of the cell, i.e., reduced resistance of the ITO and a reduced Schottky barrier at the TiO_2/ITO interface. However, the H_2-annealing step diminished the diodelike characteristics of the DSSC. Therefore, we applied an electrochemical treatment following the reduction process. The electrochemical treatment recovered the diodelike

characteristics of the DSSC by transforming Ti^{3+} defects to Ti^{4+}, and as a result, the cell efficiency increased by approximately 13%. Finally, by employing H_2-annealing and subsequent electrochemical oxidation processes, we could fabricate an ITO-based DSSC that exhibited comparable performance in comparison with an FTO-based DSSC. These findings demonstrate that the ITO-based photoelectrodes are potentially applicable to highly efficient energy conversion devices.

Acknowledgment. This work was supported by the Korea Science and Engineering Foundation (KOSEF) grant funded by the Korea government (MOST) (R01-2007-000-11075-0) (RIAM). The portion of Kookmin University was supported by the Korea Research Foundation Grant funded by the Korean Government (MOEHRD) (KRF-2007-313-D00345), and the ERC Program (CMPS, Center for Materials and Processes of Self-Assembly) of MOST/KOSEF (R11-2005-048-00000-0). This work was also supported by the Seoul R&BD program (CR070027C092852) and the research program 2008 of Kookmin University.

Supporting Information Available: Photocurrent−voltage curves for the DSSCs with the air-annealed and H_2/air-annealed ITO, thermogravimetric analysis for the TiO_2 slurry in air (black solid line) and O_2 (red dashed line) atmosphere, SEM image of interface between TiO_2 film and ITO and FTO, adsorbed dye amount of the electrode A, B, C, and D, fill factor as a function of sheet resistance, electrical properties of ITO (H_2/O_2-annealed and electrochemically treated; electrode C) and FTO (O_2-annealed; electrode D), UV−vis transmittance of ITO (H_2/O_2-annealed and electrochemically treated) and FTO (O_2-annealed). This material is available free of charge via the Internet at http://pubs.acs.org.

References and Notes

(1) O'Regan, B.; Grätzel, M. *Nature* **1991**, *353*, 737.
(2) Nazeeruddin, M. K.; Kay, A.; Rodicio, I.; Humphry, B. R.; Mueller, E.; Vlachopolous, N.; Grätzel, M. *J. Am. Chem. Soc.* **1993**, *115*, 6382.
(3) Grätzel, M. *Nature* **2001**, *414*, 338.
(4) Grätzel, M. *Inorg. Chem.* **2005**, *44*, 6841.
(5) Dittrich, T.; Beer, P.; Koch, F. *Appl. Phys. Lett.* **1998**, *73*, 1901.
(6) Schwarzburg, K.; Willig, F. *J. Phys. Chem. B* **1999**, *103*, 5743.
(7) Pichot, F.; Gregg, B. A. *J. Phys. Chem. B* **2000**, *104*, 6.
(8) Cahen, D.; Hodes, G.; Grätzel, M.; Guillemoles, J. F.; Riess, I. *J. Phys. Chem. B* **2000**, *104*, 2053.
(9) Ferber, J.; Luther, J. *J. Phys. Chem. B* **2001**, *105*, 4895.
(10) Kron, G.; Rau, U.; Werner, J. H. *J. Phys. Chem. B* **2003**, *107*, 13258.
(11) Rühle, S.; Cahen, D. *J. Phys. Chem. B* **2004**, *108*, 17946.
(12) Rühle, S.; Dittrich, T. *J. Phys. Chem. B* **2005**, *109*, 9522.
(13) Snaith, H. J.; Grätzel, M. *Adv. Mater.* **2006**, *18*, 1910.
(14) Jun, Y.; Kang, M. G. *J. Electrochem. Soc.* **2007**, *154* (1), B68.
(15) Chopra, K. L.; Major, S.; Pandya, D. K. *Thin Solid Films* **1983**, *102*, 1.
(16) Hamberg, I.; Granqvist, C. G. *J. Appl. Phys.* **1986**, *60*, R123.
(17) Tahar, R. B. H.; Ban, T.; Ohya, Y.; Takahashi, Y. *J. Appl. Phys.* **1998**, *83*, 2631.
(18) Kim, H.; Gilmore, C. M.; Pique, A.; Horwitz, J. S.; Mattoussi, H.; Murata, H.; Kafafi, Z. H.; Chrisey, D. B. *J. Appl. Phys.* **1999**, *86*, 6451.
(19) Frank, G.; Köstlin, H. *Appl. Phys. A* **1982**, *27*, 197.
(20) Ngamsinlapasathian, S.; Sreethawong, T.; Suzuki, Y.; Yoshikawa, S. *Sol. Energy Mater. Sol. Cells* **2006**, *90*, 2129.
(21) González, G. B.; Mason, T. O.; Quintana, J. P. *J. Appl. Phys.* **2004**, *96*, 3913.
(22) Kawashima, T.; Ezure, T.; Okada, K.; Matsui, H.; Goto, K.; Tanabe, N. *J. Photochem. Photobiol. A.* **2004**, *164*, 199.
(23) Yoo, B.; Kim, K.; Lee, S. H.; Kim, W. M.; Park, N.-G. *Sol. Energy Mater. Sol. Cells* **2008**, *92*, 873.
(24) Wu, N.-L.; Lee, M.-S.; Pon, Z.-J.; Hsu, J.-Z. *J. Photochem. Photobiol. A.* **2004**, *163*, 277.
(25) Suriye, K.; Praserthdam, P.; Jongsomjit, B. *Appl. Surf. Sci.* **2007**, *253*, 3849.
(26) Komaguchi, K.; Nakano, H.; Araki, A.; Harima, Y. *Chem. Phys. Lett.* **2006**, *428*, 338.
(27) Nakamura, I.; Negishi, N.; Kutsuna, S.; Ihara, T.; Sugihara, S.; Takeuchi, K. *J. Mol. Catal. A.* **2000**, *161*, 205.
(28) Weidmann, J.; Dittrich, T.; Konstantinova, E.; Lauermann, I.; Uhlendorf, I.; Koch, F. *Sol. Energy Mater. Sol. Cells* **1999**, *56*, 153.
(29) Jung, H. S.; Lee, J.-K.; Nastasi, M.; Lee, S.-W.; Kim, J.-Y.; Park, J.-S.; Hong, K. S.; Shin, H. *Langmuir* **2005**, *21*, 10332.
(30) Lee, S.; Kim, J. Y.; Youn, S. H.; Park, M.; Hong, K. S.; Jung, H. S.; Lee, J. -K.; Shin, H. *Langmuir* **2007**, *23*, 11907.
(31) Lee, S.; Kim, J. Y.; Hong, K. S.; Jung, H. S.; Lee, J.-K.; Shin, H. *Sol. Energy Mater. Sol. Cells* **2006**, *90*, 2405.
(32) Kern, R.; Sastrawan, R.; Ferber, J.; Stangl, R.; Luther, J. *Electrochim. Acta* **2002**, *47*, 4213.
(33) Han, L.; Koide, N.; Chiba, Y.; Mitate, T. *Appl. Phys. Lett.* **2004**, *84*, 2433.
(34) Hoshikawa, T.; Yamada, M.; Kikuchi, T.; Eguchi, K. *J. Electrochem. Soc.* **2005**, *152*, E68.
(35) Burnstein, E. *Phys. Rev.* **1954**, *93*, 632.
(36) Sernelius, B. E.; Berggren, K.-F.; Jin, Z.-C.; Hamberg, I.; Granqvist, C. G. *Phys. Rev.* **1988**, *37*, 10244.
(37) Moulder, J. F. *Handbook of X-ray Photoelectron Spectroscopy*; Physical Electronics, MN, 1995; p 73.
(38) Zaban, A.; Greenshtein, M.; Bisquert, J. *Chemphyschem* **2003**, *4*, 859.

JP809011A